arXiv:1612.03305v1 [astro-ph.GA] 10 Dec 2016

Radiation Pattern of Radio and Optical Components of Extended Radio Sources

V.R. Amirkhanyan[1,2]

[1]Special Astrophysical Observatory, Russian Academy of Sciences, Nizhnij Arkhyz, 369167, Russia
[2]Sternberg Astronomical Institute, M.V.Lomonosov Moscow State University, Moscow, 119992 Russia*

The relation between parameters the $D/\sqrt{I}$ and $I_C/I_{\rm SUM}$ and radiation patterns of the optical and radio components of an extended radio source is analyzed, where D and I are the apparent size and observed radiation intensity of the source or its components respectively. The parameters of the pattern in the optical and radio (1.4 GHz) ranges are estimated. The radiation pattern of extended radio-emitting regions is close to spherical and the radiation of the central component is concentrated in a 24° wide beam. Its luminosity is a factor of 4.58 higher than that of the extended component of the radio source. The radiation pattern of the optical component of the radio source turned out to be unexpectedly non-spherical: the main lobe of the pattern is about 26° wide. The g-band luminosity is 6.4–12.3 times higher than the luminosity of the spherical fraction of the "optical" radiation pattern. A list of 116 new giant radio sources is presented.

1. INTRODUCTION

Currently, the radiation pattern (RP) of a classical extended source is represented by the sum of two models of the radio sources.

(1) The Shklovsky–van der Laan model [1],[2]considers the motion of relativistic electrons in irregular magnetic fields. The radiation pattern of such a radio source is close to spherical.

(2) The model of the radiation of relativistic electrons moving in regular magnetic fields [3–6]. The radiation pattern of this structure has the form of a narrow beam, which in the simplest case of uniform magnetic field can described by the following equation [7]

$$A(\varphi) = [\gamma(1-\beta)\cos\varphi]^{-(2-\alpha)},$$

where φ is the angle between the observer's line of sight and the direction of the relativistic jet; $\gamma=(1-\beta^2)^{-1/2}$ and α is the spectral index ($S_\nu \sim \nu^{+\alpha}$). The model yields a simple formula for estimating the of the radiation pattern $\Delta\phi = 1/\gamma$, which is independent of frequency. The γ values inferred from observations of superluminal motions in radio-source jets lie in the 3–40 interval, which corresponds to $\Delta\phi$ values from 20° to 1.°5. May be that the resulting RP of the central component is equal to the sum of the patterns of different portions of the jet with different generation conditions. This conclusion is suggested by the study of the central region of Centaurus A radio source by Horiuchi et al. [8], which demonstrates the variation of the jet opening angle from 12 to 3° at the distance of 1000 to 20 000 Schwartzschield radii from the central engine. This result suggests that electrons ejected by the central engine into a wide opening angle "converge" as they move away from the center. Hence the "hedgehog" model with radial magnetic field whose RP was analyzed by Kovalev [9] applies near the central engine. In this article author performs computations over a wide frequency range, which imply that the width the RP increases with increasing frequency. For example, 1.4 GHz and 5 GHz $\Delta\phi = 13.^\circ3$ and $40.^\circ4$ at 1.4 and 5 GHz, respectively. Possibly , the truth is in a combination of models [7] and [9] as that is demanded by dialectic.

There are very few experimental estimates of the RP of extended radio sources. This include, first, the paper by Orr and Browne [10]. The above authors combined the RP from [7] with the flux density ratio of the compact and extended components (parameter $R = S_C/S_E$) and used it as the indicator of the orientation of the radio source with respect to the observer's line of sight. They further assumed equiprobable distribution of the space orientation to construct the computed distribution of parameter R and compare it with the histogram of observed R values for quasars. As a result, they estimated at 5 GHz the Lorentz factor $\gamma \sim 5$ and found the radiation level of the spherical component to be equal Such parameters imply a RP width of $\Delta\phi = 14°$. Amirkhanyan [11] used a similar method for estimating the RP, but unlike Orr and Browne [10] he investigated the statistics of the ratios of the compact component flux density to the total radio source flux density, $R_S = S_C/S_{\rm SUM}$. In addition, an upper redshift of the objects list was limited to prevent selection of the radio sources orientation with respect to the observer. As a result, the RP width was estimated to be $\Delta\phi = 42°$ and $\Delta\phi = 54°$ at 1.4 and 5 Ghz, respectively. Yet another estimate was obtained in [12] by constructing the "angular size–redshift" dependence, which yielded $\Delta\phi = 24°$ at

* Electronic address: amir@sao.ru

1.4 GHz. Complete disorder and reel.

2. OBSERVED PARAMETERS AND SPATIAL ORIENTATION OF RADIO SOURCES

To study the RP of an antenna, we change its orientation and measure its radiation. We cannot similarly manipulate with radio sources. However, we can assume that the distribution of their orientations is close to equiprobable and try to find a relation between several parameters that depend on the orientation of the radio source. Such bonds should inevitably show up if the structure of the radio source and its RP are interconnected. We assume that this condition is fulfilled.

Our conviction that $R_S = S_C/S_{\rm SUM}$ can be used as an orientation indicator is based on the assumption that RP is not spherical. The statistics of R_S from whose behavior we conclude about the form of the radiation pattern depends very strongly on the sample of radio sources, radio-telescope parameters, and eye of the observer. We therefore need yet another indicator, which inevitably depends on the parameters of the RP and orientation of the object and which can be inferred from observational data. We can then compare the behavior of these parameters with our theoretical studies ,try to find their connection and understand to which extent our assumptions are consistent with reality. To approach the truth as close as possible, we must try to "tear off" connection of our indicators from the space model.

As the first orientation indicator we use the ratio of the emission of the compact component to the total radiation intensity of the source $R_L = I_C/I_{\rm SUM}$. Note that by radiation intensity we mean the intensity in the direction of the observer. In the general case of non-spherical RP R_L is not equal to the ratio of the luminosities of the objects.

Transition to R_L allows us to eliminate the redshift dependence of the supposed orientation indicator, whereas such dependence is inevitable for $R_S = S_C/S_{\rm SUM}$: spectral indices S_C and $S_{\rm SUM}$, and hence their K corrections differ from each other.

Let us derive the formula for R_L in terms of the observed parameters of extended radio sources. Let the flux density depend on frequency as $S \propto \nu^{\alpha}$. Given that $I = Sl_b^2(z)(1+z)^{-(1+\alpha)}$, where l_b is the bolometric distance, we write

$$R_L = \frac{I_C}{I_{SUM}} = \\ = \frac{S_C l_b^2(z)(1+z)^{-(1+\alpha_C)}}{S_C l_b^2(z)(1+z)^{-(1+\alpha_C)} + S_E l_b^2(z)(1+z)^{-(1+\alpha_E)}}.$$

Here α_E and S_E are the spectral index and flux density of the extended component, respectively, and α_C and S_C are the spectral index and flux density of the compact component, respectively. Given that $S_E = S_{\rm SUM} - S_C$, we derive, after simple transformations, the following formula

$$\begin{aligned} R_L &= \frac{S_C}{S_C + S_{\rm SUM} - S_C(1+z)^{\alpha_C - \alpha_E}} \\ &= \frac{(1+z)^{\alpha_E - \alpha_C}}{(1+z)^{\alpha_E - \alpha_C} + \dfrac{1}{R_S} - 1}. \end{aligned} \quad (1)$$

The second parameter

$$T = \frac{D}{\sqrt{I}}, \quad (2)$$

where $D = D_0 \sin\varphi$ is the visible size of the radio source and $I = I_0\, A(\varphi)$, the visible radiation of the radio source or its component. The word "visible" is used to indicate that both D and I depend on the orientation of the radio source relative to the observer; φ is the angle between the line of sight and the direction toward the maximum of emission of the radio source; D_0 is the true size of the radio source and I_0 is the radiation in the direction of the maximum of the radiation pattern $A(\varphi)$. The T value can be easily computed from the observed parameters

$$T = \frac{\Theta}{\sqrt{S}}(1+z)^{-\frac{(3-\alpha)}{2}} \quad (3)$$

and does not depend on the model of space. Θ is the angular size of the radio source and S, the flux density of the radio source or of its component.

The author assumes that substituting the flux density of the entire radio source or some of its components (compact, extended, optical) into the denominator in formula (3) will make it possible to estimate the parameters of the RP of both the entire radio source and its corresponding fractions.

Let us relate R_L and T via RP $A(\varphi)$. Consider the canonical model of a radio source with symmetric two-sided components [7, 10]. Let the ideal RP of such object be axisymmetric with respect to the jet axis and have two symmetric maxima in opposite directions. Let us adopt the description of the radiation pattern from [11]

$$A(\varphi) = \frac{I}{I_0} = a + (1-a)\cos^{2n}\varphi. \quad (4)$$

Here a is the level of the spherical component of the RP and n, a parameter that determines the width of the main lobe of the RP. If $n = 0$ then the RP degenerates into a spherical pattern ($A(\varphi) = 1$).

Let us now determine the relation between R_L and the orientation of the radio source relative to the observer

$$R_L = \frac{I_C}{I_{\rm SUM}} = \frac{(1-a)\cos^{2n}\varphi}{a + (1-a)\cos^{2n}\varphi}. \quad (5)$$

It is evident from this equation that $R_L < 1 - a$.

Let us now extract the following relation from formula (5)

$$\cos\varphi = \left[\frac{aR_L}{(1-a)(1-R_L)}\right]^{\frac{1}{2n}}$$

and, given that $D = D_0 \sin\varphi$, substitute it into formula (2). As a result, we obtain the following computed dependence of T on R_L for different components of the radio source:

(1) The total radiation of the radio source

$$\begin{aligned} T_{\rm SUM} &= \frac{D}{\sqrt{I}_{\rm SUM}} = \frac{D_0\sin\varphi}{\sqrt{I_0[a+(1-a)\cos^{2n}\varphi]}} \\ &= \frac{D_0\sqrt{1-\left[\dfrac{aR_L}{(1-a)(1-R_L)}\right]^{\frac{1}{n}}}}{\sqrt{\dfrac{aI_0}{1-R_L}}}; \end{aligned} \quad (6)$$

(2) The compact component of the radio source

$$\begin{aligned} T_C &= \frac{D}{\sqrt{I}_C} = \frac{D_0\sin\varphi}{\sqrt{I_0(1-a)\cos^{2n}\varphi}} \\ &= \frac{D_0\sqrt{1-\left[\dfrac{aR_L}{(1-a)(1-R_L)}\right]^{\frac{1}{n}}}}{\sqrt{I_0\dfrac{aR_L}{1-R_L}}}; \end{aligned} \quad (7)$$

(3) the extended component of the radio source

$$\begin{aligned} T_E &= \frac{D}{\sqrt{I}_E} = \frac{D_0\sin\varphi}{\sqrt{aI_0}} \\ &= \frac{D_0\sqrt{1-\left[\dfrac{aR_L}{(1-a)(1-R_L)}\right]^{\frac{1}{n}}}}{\sqrt{aI_0}}. \end{aligned} \quad (8)$$

Formulas (6)–(8) include parameters of the RP and therefore there is hope that these parameters can be estimated by comparing the model with experiment. Note that all the three equations must demonstrate the agreement with the experiment for the same parameters of RP.

The optical object is a component of the radio source and we can extend the above reasoning to it in order to estimate the RP in the optical range. We now consider the general case allowing non-spherical radiation of the optical component. We further assume that the optical radiation is associated with the structure of the radio source: the symmetry axis of the optical radiation coincides with the jet axis. It follows from the canonical model of the radio source, which assume the synchrotron mechanism of jet radiation over a wide range of wavelengths and the closeness of the spatial orientation of the rotation axes of the host galaxy and the jet. Here we can draw upon the works by Condon et al. [13] and Browne and Battye [14], who showed based on experimental data that the the distribution function of the difference of the position angles radio sources and of elliptical galaxies identified with them is has maximum near 90°. Hence the position angle of the minor axis, which is close to the position angle of the normal to the galaxy, coincides with the orientation of the radio jet. Let the form of the optical RP be described by formula (4), but with its proper values of $n_{\rm opt}$ and $a_{\rm opt}$:

$$A_{\rm opt}(\varphi) = \frac{I_{\rm opt}}{I_{0,\,\rm opt}} = a_{\rm opt} + (1-a_{\rm opt})\cos^{2n_{\rm opt}}\varphi \quad (4')$$

Currently, we cannot separate the radiation into the extended and compact fractions of the optical object. We therefore use formula (6) for the total radiation, where we leave parameter R_L determined from radio data as the orientation indicator, but replace RP (4) by formula (4′). We then have

$$\begin{aligned} T_{\rm opt} &= \frac{D}{\sqrt{I}_{\rm opt}} = \frac{D_0\sin\varphi}{\sqrt{I_{0,\,\rm opt}[a_{\rm opt}+(1-a_{\rm opt})\cos^{2n_{\rm opt}}\varphi]}} \\ &= \frac{D_0\sqrt{1-\left[\dfrac{aR_L}{(1-a)(1-R_L)}\right]^{\frac{1}{n}}}}{\sqrt{I_{0,\,\rm opt}\left[a_{\rm opt}+(1-a_{\rm opt})\dfrac{aR_L}{(1-a)(1-R_L)}\right]^{\frac{n_{\rm opt}}{n}}}}. \end{aligned} \quad (9)$$

3. SAMPLES OF RADIO SOURCES

To compare formulas (6)–(9) with real measurements, we used two lists of extended radio sources:

(1) Sample of objects whose apparent size does not exceed 0.7 Mpc in the ΛCDM model. This list includes 2947 identified radio sources from Amirkhanyan [15]. For each of these objects its angular size, total flux density, component flux densities, redshift, and g-band magnitude of the optical counterpart are known.

(2) Objects whose apparent sizes exceed 0.7 Mpc. This sample contains 254 giant radio sources from catalogs [15**?** –25].

The list does not include objects with photometric redshifts. To ensure uniformity of parameter determination, we found all objects in the NVSS (`http://www.cv.nrao.edu/nvss/NVSSlist.shtml`) or SUMSS (`http://www.astrop.physics.usyd.edu.au/sumsscat/sumsscat.Feb-16-2012`) catalogs. We thereby determined the flux densities and coordinates of the radio-source components, and

also their angular sizes measured as the separation between the most spaced components.

If there was a radio component within 10–15″ of the optical component then this radio component was considered to be the central one and S_C was set equal to its flux density. If no central component was present then its flux density was assigned as $S_C = 0.1$ mJy, which is below the detection threshold for NVSS. The data of the FIRST survey (`http://sundog.stsci.edu/cgi-bin/searchfirst`) were used to refine the coordinates of the central components if the radio source was located in the area covered by this survey.

We further added to the list 92 radio sources found in the NVSS catalog using the software developed by the author [25] (see Table below). This table also includes the "giants" from [15]. The author broke selection criteria for the radio source $2057 + 0012$, because its extent exceeds the formal 0.63 Mpc because of its complex shape.

List of giants

α_{2000}	δ_{2000}	Angular size, arcsec	Total flux density, mJy	Flux density of the central component, mJy	g-band magnitude of the optical component	z	Apparent size, Mpc	Object type
(1)	(2)	(3)	(4)	(5)	(6)	(7)	(8)	(9)
				NVSS				
00 03 31.50	+03 51 11.0	1174.7	470.6	10.9	17.11	0.097	2.08	Gal
00 17 47.80	−22 23 20.0	386.5	485.6	0.1	17.40	0.108	0.75	Gal
00 20 32.90	−20 16 13.0	490.5	965.8	207.6	18.80	0.197	1.58	Gal
00 37 19.10	+26 13 12.0	435.1	156.0	119.4	17.43	0.148	1.12	Gal
00 43 59.80	+31 37 20.0	159.9	129.3	11.3	17.85	0.631	1.09	QSO
01 20 38.60	−17 01 55.0	505.1	310.4	81.5	17.22	0.089	0.83	Gal
01 43 56.00	+06 24 38.0	268.8	134.9	29.3	17.99	0.180	0.81	Gal
01 55 46.30	−26 54 04.8	220.4	22.7	8.3	17.27	0.209	0.75	Gal
02 49 36.80	−20 30 11.0	480.0	1020.6	0.1	16.96	0.087	0.77	Gal
02 51 46.80	+15 50 13.0	131.8	763.7	30.1	17.58	0.489	0.79	QSO
03 11 51.70	−31 30 01.0	106.3	1052.0	780.3	20.51	2.420	0.88	QSO
03 13 32.90	−06 31 58.0	177.3	164.8	0.1	19.50	0.389	0.93	Gal
04 22 21.00	+15 10 59.0	735.0	168.8	6.7	18.10	0.409	3.98	Gal
07 46 33.70	+17 08 10.0	436.5	81.2	16.7	19.21	0.188	1.36	Gal
07 53 41.30	+34 30 32.0	252.8	111.7	11.6	23.59	0.548	1.61	Gal
08 24 01.00	+24 47 36.0	301.2	39.0	0.1	19.14	0.224	1.08	Gal
08 32 34.10	+04 24 36.0	446.8	191.9	112.5	15.95	0.106	0.86	Gal
08 41 45.90	−25 38 18.0	619.9	76.8	22.0	14.68	0.083	0.95	Gal
08 45 25.51	+52 29 15.9	211.7	41.9	20.1	20.74	0.403	1.14	Gal
08 48 36.10	+05 55 23.0	157.4	1319.5	87.0	19.06	0.798	1.18	Gal
08 57 01.76	+01 31 30.9	276.3	96.3	8.1	20.25	0.273	1.15	Gal
09 11 54.60	+08 12 31.0	203.6	347.8	86.3	18.64	0.243	0.77	Gal
09 12 36.60	+68 34 25.0	290.6	425.4	396.6	18.69	1.080	2.38	Gal
09 14 19.50	+10 06 41.0	366.1	469.8	348.7	19.80	0.311	1.65	Gal
09 32 38.30	+16 11 57.0	236.7	748.9	1.2	18.43	0.191	0.75	Gal
09 40 03.80	+51 04 22.0	240.7	254.7	16.3	18.87	0.207	0.81	Gal
09 54 19.19	+27 15 59.9	186.7	150.5	11.0	20.65	0.471	1.10	Gal
10 14 43.92	−01 46 12.0	240.8	225.0	31.7	18.02	0.198	0.78	Gal
10 17 18.70	+39 31 21.0	125.9	745.4	13.6	20.20	0.530	0.79	Gal
10 36 23.00	+38 31 31.1	185.0	128.8	2.7	20.36	0.408	1.00	Gal
10 48 04.80	+74 19 40.0	643.5	69.2	0.1	17.29	0.121	1.39	Gal
11 00 38.30	−02 34 37.0	227.7	71.8	41.0	21.39	0.399	1.21	Gal
11 04 46.99	+21 03 17.7	237.0	108.1	7.7	18.53	1.153	1.96	QSO
11 18 59.17	+27 54 49.5	180.9	523.0	0.1	20.48	0.317	0.83	Gal
11 47 20.70	−12 53 10.0	125.0	364.4	0.1	16.93	0.497	0.76	Gal
11 48 55.90	−04 04 10.0	190.3	613.9	175.3	17.17	0.340	0.91	QSO
11 53 18.00	+03 38 05.0	170.9	52.7	5.8	20.71	0.328	0.80	Gal
11 56 54.70	+26 32 32.0	271.6	168.9	124.2	18.09	0.156	0.72	Gal
11 59 26.20	+21 06 56.0	156.9	270.2	21.2	17.27	0.349	0.77	QSO
12 02 40.30	−12 51 40.0	198.3	131.8	93.4	16.56	0.553	1.27	QSO
12 13 57.10	+08 32 02.0	158.2	45.6	13.7	17.87	0.811	1.20	QSO
12 48 13.90	+36 24 24.0	251.0	90.5	2.9	18.13	0.207	0.84	Gal
12 55 50.13	+58 18 42.0	216.4	34.7	12.8	20.52	0.361	1.08	Gal
13 13 57.70	+64 25 55.0	248.6	78.0	0.1	18.99	0.221	0.88	Gal
13 14 03.40	−33 03 56.0	185.4	233.6	95.1	19.43	0.484	1.11	QSO
13 14 43.80	+27 37 41.0	236.9	30.1	5.9	20.93	0.418	1.30	Gal
13 20 41.10	+45 51 23.0	306.7	84.1	12.5	17.93	0.178	0.91	Gal
13 28 34.10	−01 29 18.0	308.4	354.4	15.6	17.91	0.151	0.80	Gal
13 28 34.40	−03 07 45.0	804.7	207.5	12.6	17.49	0.085	1.27	Gal
13 45 57.50	+54 03 17.0	259.4	346.0	9.3	18.35	0.163	0.72	Gal
13 50 36.10	−16 34 50.0	1153.3	300.3	109.2	16.60	0.098	2.06	QSO
13 53 35.92	+26 31 47.5	158.0	239.6	55.3	16.87	0.310	0.71	QSO
14 06 26.00	+45 09 05.0	263.6	44.2	2.2	20.85	0.400	1.41	Gal
14 22 49.20	−27 27 56.0	102.8	2418.2	2268.8	17.60	0.985	0.82	QSO
14 30 45.66	+14 50 38.0	259.5	72.0	5.2	16.41	0.377	1.33	QSO

(Cont.)

α_{2000}	δ_{2000}	Angular size, arcsec	Total flux density, mJy	Flux density of the central component, component	g-band magnitude of the optical	z	Apparent size, Mpc	Object type
(1)	(2)	(3)	(4)	(5)	(6)	(7)	(8)	(9)
14 31 51.10	+10 29 59.0	270.4	61.8	18.5	18.11	0.166	0.76	Gal
14 32 44.90	+30 14 35.0	183.9	75.4	50.6	18.81	0.355	0.91	QSO
14 41 24.00	−34 56 46.0	156.7	419.6	395.1	17.43	1.159	1.30	QSO
14 47 10.20	+22 10 07.6	197.7	49.3	0.1	18.99	0.249	0.77	Gal
14 49 54.80	+14 06 11.0	298.1	133.1	7.7	21.98	0.251	1.16	Gal
14 51 06.40	+53 33 54.0	187.9	42.5	2.6	19.07	0.432	1.05	Gal
15 13 44.90	−10 12 00.0	228.5	1062.8	874.5	18.40	1.513	1.95	QSO
15 18 30.90	+48 32 14.0	108.0	66.4	5.1	18.35	0.576	0.71	QSO
15 24 44.60	+19 59 57.0	247.3	25.8	0.1	20.39	0.345	1.20	Gal
15 29 18.00	+32 48 42.0	298.1	65.7	32.4	17.75	1.650	2.55	QSO
15 29 50.80	+02 25 15.0	163.3	88.1	7.3	20.63	0.339	0.78	Gal
15 40 56.80	−01 27 10.0	275.1	214.9	10.3	17.78	0.149	0.71	Gal
15 48 16.70	+69 49 35.0	204.2	272.7	33.1	16.65	0.375	1.05	QSO
15 52 06.67	+22 47 39.5	667.3	545.5	5.7	17.42	0.116	1.39	Gal
15 52 22.70	+22 33 12.0	672.9	265.5	7.3	15.72	0.068	0.86	Gal
16 03 34.10	+36 59 52.0	155.9	45.8	9.5	18.40	0.967	1.24	QSO
16 09 53.40	+43 34 11.0	123.9	337.1	9.5	17.61	0.760	0.91	QSO
16 22 06.00	+24 49 16.0	334.2	58.7	5.0	18.41	0.148	0.86	Gal
16 23 42.40	+25 21 47.0	283.0	226.3	68.1	21.50	0.364	1.42	Gal
16 49 28.90	+30 46 52.0	108.4	110.6	39.7	18.62	1.125	0.89	QSO
17 52 46.00	+17 34 20.0	139.0	370.6	341.3	18.10	0.504	0.85	QSO
19 21 14.00	+48 06 19.0	519.4	1097.9	0.1	12.27	0.102	0.96	Gal
20 57 20.40	+00 12 07.0	267.7	406.4	74.9	17.85	0.135	0.63	Gal
21 45 04.50	−06 59 08.0	341.8	160.0	9.7	19.60	0.315	1.56	Gal
22 25 13.60	−16 19 04.0	626.2	547.8	0.1	16.05	0.103	1.17	Gal
22 30 40.30	−39 42 52.0	191.3	644.3	320.1	17.38	0.318	0.88	QSO
22 34 58.80	−02 24 18.0	192.1	73.6	24.8	18.55	0.550	1.23	QSO
22 41 01.99	+27 32 59.0	269.4	258.3	51.5	17.43	0.493	1.63	QSO
22 53 36.00	−34 55 31.0	257.8	280.0	50.0	17.83	0.212	0.88	Gal
23 16 00.60	−28 23 53.0	437.9	319.2	5.6	18.18	0.229	1.59	Gal
23 21 54.80	−24 25 52.0	179.4	43.5	10.1	18.21	0.279	0.76	Gal
23 33 12.40	+00 5658.5	890.4	87.3	0.1	16.43	0.087	1.43	Gal
23 33 55.24	−23 43 40.7	1189.9	1118.5	782.1	13.82	0.048	1.10	Gal
23 45 33.10	−04 48 54.6	1003.6	161.6	0.1	15.72	0.075	1.41	Gal
23 55 24.70	+26 24 14.0	195.9	316.0	14.8	19.44	0.240	0.74	Gal
				FIRST				
08 38 13.13	+13 58 10.7	127.9	59.9	3.7	18.72	2.024	1.08	QSO
09 42 16.50	+12 45 03.6	93.0	46.6	12.0	19.09	1.432	0.79	QSO
10 17 54.86	+47 05 29.0	116.1	25.2	7.8	18.69	0.668	0.81	QSO
10 20 03.00	−02 47 18.0	95.0	88.5	6.7	20.53	1.447	0.81	QSO
10 38 22.47	+13 46 57.0	101.0	72.2	65.6	17.66	0.947	0.80	QSO
10 56 37.96	+27 43 43.8	94.2	316.5	15.4	20.49	0.998	0.76	QSO
11 09 35.40	+51 04 02.6	92.4	30.2	3.1	19.48	1.179	0.77	QSO
11 12 15.45	+11 29 19.3	108.4	74.0	7.7	19.15	1.132	0.90	QSO
12 08 22.00	+22 19 58.2	108.8	135.0	7.9	18.45	0.745	0.80	QSO
12 14 31.15	+18 28 15.1	89.8	100.6	17.7	20.58	1.590	0.77	QSO
12 57 10.80	+40 54 29.2	119.5	29.5	2.9	19.30	1.067	0.98	QSO
13 33 07.00	+04 50 48.5	129.5	48.0	6.3	18.50	1.405	1.10	QSO
13 56 00.04	+19 04 20.8	90.8	36.0	12.5	18.62	2.224	0.76	QSO
14 15 54.37	+49 09 21.2	89.8	25.6	12.0	19.60	1.371	0.76	QSO
14 37 47.74	+07 48 56.2	139.5	56.0	3.1	18.78	1.472	1.19	QSO
14 39 32.68	+45 50 28.3	127.1	21.7	3.2	19.24	1.836	1.08	QSO
14 46 26.80	+41 33 18.0	102.8	496.2	3.0	20.44	0.675	0.72	Gal
14 50 38.83	+45 49 54.6	93.0	93.8	9.2	19.46	1.622	0.80	QSO
14 51 03.23	+11 41 08.6	88.3	37.6	13.2	18.44	1.067	0.72	QSO
14 53 08.00	+22 17 07.7	115.9	103.4	15.8	19.74	0.785	0.87	QSO
15 07 39.50	+11 04 03.7	140.8	226.4	8.8	18.02	0.475	0.83	QSO
15 33 13.22	+06 58 01.6	95.6	45.6	33.6	18.23	1.160	0.79	QSO
15 49 33.46	+00 47 32.6	84.2	20.2	12.0	19.52	1.253	0.71	QSO
16 01 51.57	+17 54 10.2	104.6	166.6	5.6	18.27	0.660	0.73	QSO
16 23 46.42	+27 35 13.6	93.8	63.6	57.5	18.82	1.397	0.80	QSO
23 56 06.32	−01 31 51.2	98.2	190.5	6.1	22.23	1.028	0.80	Gal

4. DETERMINATION OF THE PARAMETERS OF THE RADIATION PATTERN

4.1. The First Sample, $D < 0.7$ Mpc

For all radio sources we determine parameter R_L by formula (1). Figure 1 shows the relation between R_L and R_S. The dashed line shows the identity relation $R_L = R_S$. The lower boundary of the plot (the solid line) was computed by formula (1) for $z = 3.7$ (the maximum redshift in the sample). We adopted the same spectral indices for all radio sources be-

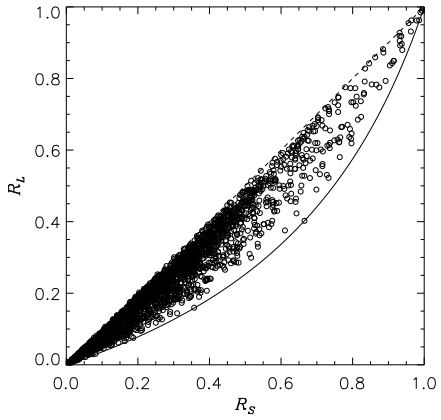

Figure 1. Relation between R_L and R_S for the radio sources of the first list. The dashed line shows the $R_L = R_S$ relation. The lower boundary of the plot (the solid line) was computed by formula (1) for $z = 3.7$ (maximum redshift in this sample).

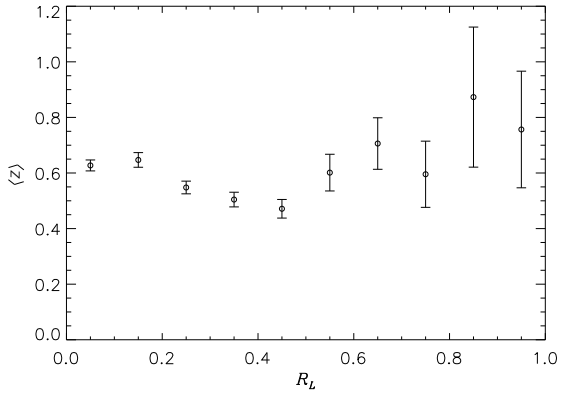

Figure 2. Dependence of z on R_L for radio sources with apparent sizes $D < 0.7$ Mpc. We subdivided the entire range of R_L values into ten equal bins. In each bin we computed the mean redshift by averaging the z values of the objects and the corresponding standard deviation.

cause these data are unavailable for most of the radio sources. We set $\alpha_E = -0.8$ and $\alpha_C = -0.1$ for extended and compact components, respectively. The eventual selection by redshift appears to be small because the average z of radio sources weakly depends on R_L (Fig. 2).

We now determine parameter T for different radio-source components by substituting into formula (3) the total flux densities $S_{\rm SUM}$, flux densities S_C of the central fraction, or flux densities S_E of external components. Figs. 3a, 3b, and 3c show the plots $T_{\rm SUM}$, T_C, and T_E as functions of R_L for objects of the first sample.

The distribution functions of the true sizes and true luminosities of extended radio sources do not depend on their spatial orientation and therefore the upper boundary of parameter T as a function of R_L is determined by the RP of radio sources (formulas (6)–(8)). When computing the upper limit (the solid line in Figs. 3a–3c) we set the maximum true sized of radio sources equal to $D_0 = 0.7$ Mpc.

We then varied a, n, and I_0 to determine the parameter values that allow achieving the best agreement between the computed and visible boundaries simultaneously in three plots: $a = 0.007$, $n = 15$, $I_0 = 10^{25}$ W Hz^{-1} sr^{-1}.

The normalization of RP (4) differs from traditional 4π:

$$N = 4\pi \left(a + \frac{1-a}{2n+1} \right), \qquad (10)$$

and is equal to 0.49 for the inferred RP parameters. Hence the minima, luminosity of the radio sources of the sample is $N \times I_0 = 4.9 \times 10^{24}$ W Hz^{-1}.

The dashed line in Figs. 3a and 3c demonstrate the sensitivity of the computed upper boundaries for parameter values from $a = 0.005$ to $a = 0.009$. For the same purpose we show by the dashed line in Fig. 3b the boundary for $n = 12$ and $n = 18$. Figures 3a, 3b and 3c clearly demonstrate that the RP of the extended source is evidently non-spherical. Its main lobe whose maximum coincides with the major axis of the radio source has the width of about 24°. The distribution of the radiation of outer components is close to spherical and its level is 140 times lower than the intensity at the maximum and the luminosity of the compact component is a factor of 5.48 higher than that of outer components.

Before computing parameter T of the optical component we must decide how to compute the K-correction for the AGN. The K-correction is usually viewed as a magnitude correction. Here we define it as the g-band flux density correction for the optical component of the radio source. To determine the K-correction, we used the most complete and homogeneous photometric measurements in the u-, g-, r-, i-, and z-filters from the SDSS-survey[1]. For 540 objects with redshifts greater than 1 we supplemented these data with infrared photometry from the 2MASS (J-, H-, and K-filters) [26] and WISE All-sky ($W1$-filter) survey [27]. We then constructed the spectrum of the optical component based on the entire set of photometric data and determined the K-correction.

To compute $T_{\rm opt}$ we rewrite equation (3) taking into account the inferred K-correction :

$$T_{\rm opt} = \frac{\Theta}{\sqrt{S_g K_{\rm COR}}} (1+z)^{-2}. \qquad (11)$$

[1] http://skyserver.sdss.org/dr12/en/tools/crossid/crossid.aspx.

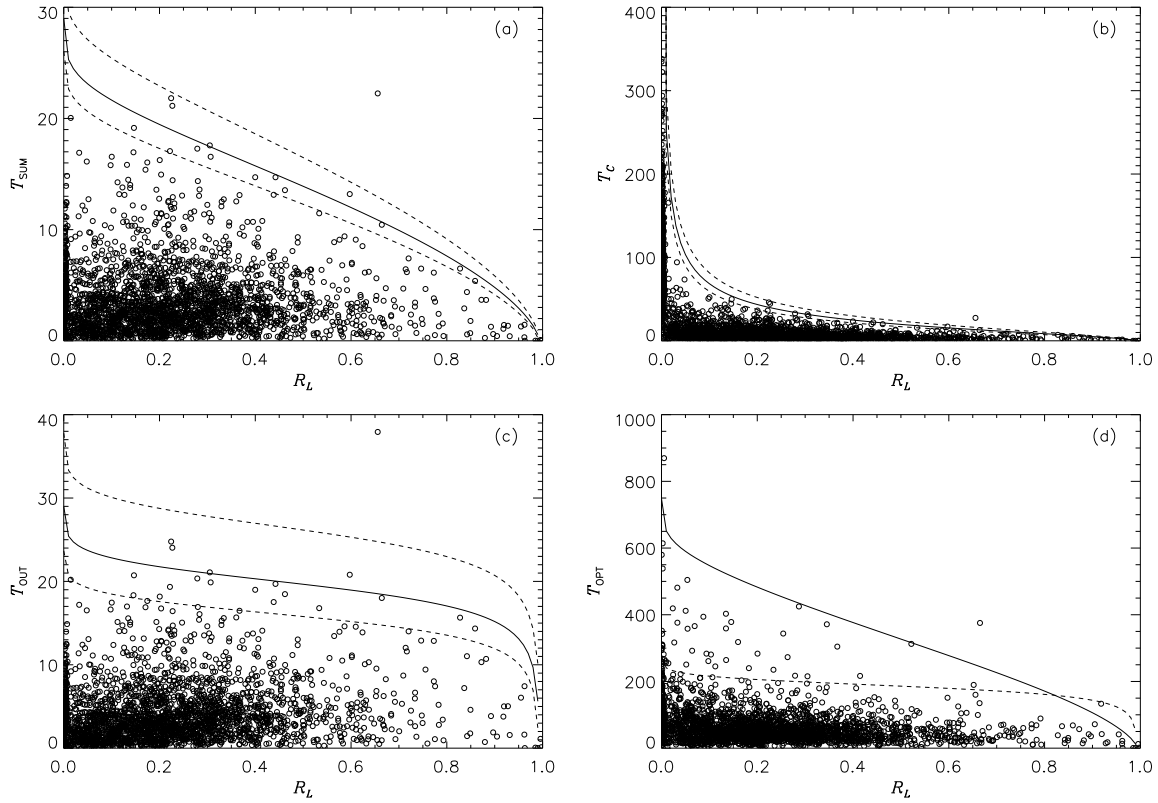

Figure 3. Radio sources with apparent sizes smaller than 0.7 Mpc. Dependence on R_L: (a) $T_{\rm SUM}$, (b) T_C, (c) T_E, (d) $T_{\rm opt}$. The solid line in Figs. (a), (b), and (c) shows the upper limit computed by formulas (6)–(8) for the optimum parameters of the RP of the radio source: $a = 0.007$, $n = 15$. The upper limit in Fig. (d) is computed by formula (9) for the parameters of the RP of the optical component $a_{\rm opt} = 0.005$, $n_{\rm opt} = 15$. The dashed line shows the boundary of spherical RP.

Here S_g is the observed flux density of the object in the g-band filter. We show the results of computations in Fig. 3d. Unexpectedly, the plot showed that the RP of the optical component of the radio source is far from spherical. The solid line shows the optimum upper boundary for $a_{\rm opt} = 0.005$, $n_{\rm opt} = 15$, $I_{0,\,\rm opt} = 2 \times 10^{22}$ W Hz^{-1} sr^{-1} . The dashed line shows where the boundary should be in the case of spherical RP in the optical range with intensity $I_{0,\,\rm opt}$.

4.2. *Second Sample, $D > 0.7$ Mpc*

The computations performed for objects of the first sample were repeated for the giant radio sources of the second sample. Figures 4a, 4b, 4c, and 4d show the results of computations for $T_{\rm SUM}$, T_C, T_E, and $T_{\rm opt}$ (the open circles). The boundary of the distribution was computed for $a = 0.007$, $n = 15$, $I_0 = 1.5 \times 10^{25}$ W Hz^{-1} sr^{-1}, $D_0 = 2.8$ Mpc. It is evident that because of the limited statistics the agreement with experimental data is not so good as in the case of the first sample. It is, however, evident that the RP of giant radio sources is also non-spherical and its parameters are close to those inferred for the first list. To demonstrate the latter statement, we added to Fig. 4b objects from Fig. 3b (the filled circles). To cover the wide range of T_C and R_L values, the figure is plotted in logarithmic scale. The relative shift of the boundaries of the first and second samples along the vertical axis (the dashed and solid lines, respectively) is primarily determined by the change of the true maximum size of radio sources and not the parameters of the RP. We could find photometry in the SDSS catalog for computing $T_{\rm opt}$ (Fig. 4d) only for 146 giant radio sources. We compiled the $BVRIJHK$ photometry from VizieR database[2]. This allowed us to determine the g-band flux density and the corresponding K-correction reduced to this band for 254 objects. The boundary was computed for the following parameter values: $a_{\rm opt} = 0.003$, $n_{\rm opt} = 13$, $I_{0,\,\rm opt} = 3 \times 10^{22}$ W Hz^{-1} sr^{-1}, $D_0 = 2.8$ Mpc

[2] http://vizier.u-strasbg.fr/viz-bin/VizieR.

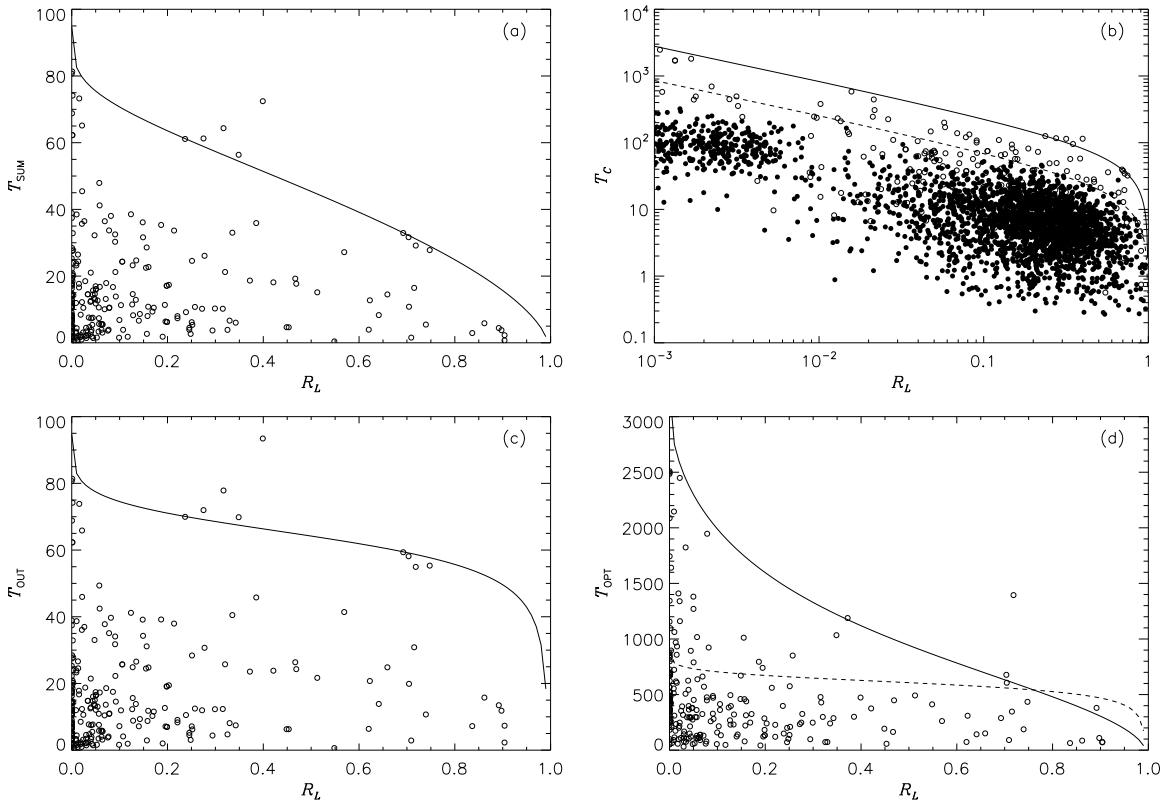

Figure 4. Radio sources with apparent sizes greater than 0.7 Mpc. Dependence on R_L: (a) $T_{\rm SUM}$, (b) T_C, (c) T_E, (d) and $T_{\rm opt}$. The solid line in Figs. a, b, c shows the upper limit computed by formulas (6)–(8) for parameters of the radio-source RP $a = 0.007$, $n = 15$. The dashed line in (b) shows, for comparison, the boundary of objects of the first list (the filled circles). The upper boundary in (d) was computed by formula (9) for parameters of the RP of the optical component $a_{\rm opt} = 0.003$, $n_{\rm opt} = 13$. The dashed line shows the boundary of the spherical RP.

(Fig. 4d).

The dashed line in the same figure shows where the boundary should be if the RP in the optical is spherical and $I_{0,\,\rm opt} = 3 \times 10^{22}$ W Hz^{-1} sr^{-1}. It follows from these parameters that the FWHM of the main lobe of the optical RP is 26.̊4.

5. CONCLUSIONS

It can be concluded from the above that:

(1) The ratio of the radiation of the compact component to total radiation of the extendet radio source is indeed connects with its spatial orientation.

(2) The form of the RP does not depend on the size or luminosity of the radio source. This may also be true for objects with luminosities higher than $L = 4.9 \times 10^{24}$ W Hz^{-1}.

(3) The central component emits within a narrow beam whose width at 1.4 GHz is of about 24°. This value corresponds to $\gamma = 2.33$.

(4) The RP of the extended component is close to spherical, its level is about 0.005–0.01 of the intensity at the maximum, and its luminosity is equal to 0.13–0.24 that of the entire radio source.

(5) The RP of the optical component of the radio source is also non-spherical, its radiation is concentrated within a beam of width 24–27°, and the level of the spherical component is of about 0.003–0.005 of the intensity at the maximum.

ACKNOWLEDGMENTS

This research has made use of the VizieR catalogue access tool, CDS, Strasbourg, France.

1. I. S. Shklovskii, Astronom. Zh.**42**, 30 (1965).

2. H. van der Laan, Nature (London) **211**, 1131 (1966).

3. M. J. Rees, Nature (London) **211**, 468 (1966).
4. L. M. Ozernoy and V. N. Sazonov, Astrophys. and Space Sci. **3**, 365 (1969).
5. V. N. Kuril'chik, Astronom. Zh.**48**, 684 (1971).
6. Y. A. Kovalev and V. P. Mikhailutsa, Sov. Astronom.**24**, 400 (1980).
7. P. A. G. Scheuer and A. C. S. Readhead, Nature (London) **277**, 182 (1979).
8. Y. Y. Kovalev, Astronom. Zh.**71**, 846 (1994).
9. S. Horiuchi, D. L. Meier, R. A. Preston, and S. J. Tingay, Publ. Astronom. Soc. Japan**58**, 211 (2006).
10. M. J. L. Orr and I. W. A. Browne, Monthly Notices Roy. Astronom. Soc. **200**, 1067 (1982).
11. V. R. Amirkhanyan, Astronom. Zh.**70**, 16 (1993).
12. V. R. Amirkhanyan, Astrophysical Bulletin**69**, 383 (2014).
13. J. J. Condon, D. T. Frayer, and J. J. Broderick, Astronom. J. **101**, 362 (1991).
14. I. W. A. Browne and R. A. Battye, ASP Conf. Ser. **427**, 365 (2010).
15. V. R. Amirkhanyan, Astrophysical Bulletin**64**, 333 (2009).
16. K. Nilsson, M. J. Valtonen, J. Kotilainen, and T. Jaakkola, Astrophys. J. **413**, 453 (1993).
17. L. Lara, W. D. Cotton, L. Feretti, et al., Astron. Astrophys., **370**, 409 (2001).

17. L. Lara, I. Márquez, W. D. Cotton,et al.,Astronom. and Astrophys.**378**, 826(2001).
18. C. H. Ishwara-Chandra and D. J. Saikia, Monthly Notices Roy. Astronom. Soc. **309**, 100 (1999).
19. A. P. Schoenmakers, A. G. de Bruyn, H. J. A. Röttgering, and H. van der Laan, Astronom. and Astrophys. **374**, 861 (2001).
20. J. Machalski, M. Jamrozy, and S. Zola, Astronom. and Astrophys. **371**, 445 (2001).
21. J. Machalski, M. Jamrozy, S. Zola, and D. Koziel, Astronom. and Astrophys. **454**, 85 (2006).
22. K. Chyży, M. Jamrozy, S. J. Kleinman, et al., Baltic Astronomy **14**, 358 (2005).
23. A. Buchalter, D. J. Helfand, R. H. Becker, and R. L. White, Astrophys. J. **494**, 503 (1998).
24. L. Saripalli, R. W. Hunstead, R. Subrahmanyan, and E. Boyce, Astronom. J. **130**, 896 (2005).
25. V. R. Amirkhanyan, V. L. Afanasiev, and A. V. Moiseev, Astrophysical Bulletin**70**, 45 (2015).
26. R. M. Cutri, M. F. Skrutskie, S. van Dyk, et al., VizieR Online Data Catalog **2246** (2003).
27. R. M. Cutri, et al., VizieR Online Data Catalog **2328** (2014).